APPLIED SCIENCES AND ENGINEERING

Density fluctuations in granular piles traversing the glass transition: A grain-scale characterization via the internal energy

Paula A. Gago[1]* and Stefan Boettcher[2]

The transition into a glassy state of the ensemble of static, mechanically stable configurations of a tapped granular pile is explored using extensive molecular dynamics simulations. We show that different horizontal subregions ("layers") along the height of the pile traverse this transition in a similar manner but at distinct tap intensities. We supplement the conventional approach based purely on properties of the static configurations with investigations of the grain-scale dynamics by which the tap energy is transmitted throughout the pile. We find that the effective energy that particles dissipate is a function of each particle's location in the pile and, moreover, that its value plays a distinctive role in the transformation between configurations. This internal energy provides a "temperature-like" parameter that allows us to align the transition into the glassy state for all layers, as well as different annealing schedules, at a critical value.

INTRODUCTION

Granular materials are ubiquitous in nature and have always fascinated scientists, Coulomb and Reynolds among them, due to their somewhat counterintuitive behavior (*1*). They have been considered as an additional state of matter in its own right (*2*) and although they are the second-most common form by which mankind handles materials (behind fluids), the way in which mechanical perturbations define its macroscopic properties are still not well understood. One of their key characteristic is that they tend to be at rest: Any input of energy provided to the system, whether by tapping, shearing, or tilting, is eventually dissipated through frictional contacts and collisions among the grains. Specifically, it requires such an external input of energy to be able to modify its configuration. Thus, the way in which the system behaves (fluid, solid, and gas) is strongly determined by the way this external energy is dispensed and the microscopic processes leading to its dissipation. Attributes such as friction, density, the granular contact network, container geometry, etc., will likely play a role in this process.

Although their propensity to stay at rest marks these materials as "athermal," any boundary making it distinct from other, thermal states of matter are progressively weakening. For example, we have recently described the transition of a tapped granular pile into a glassy state (*3*) familiar from polymers, complex fluids, and frustrated magnets (*4*–*9*). For these disordered thermal materials, relaxation times increase for many orders of magnitude (and possibly even diverge) over a small range of temperatures (*5*), beyond which the systems remains out of equilibrium for any practical purpose. Whether the transition was approached gradually or via a hard-quench in the intensity of taps, we encountered the same phenomenology in the granular pile as is observed for other glass-forming materials. Although the distribution of fluctuations elicited by a perturbation within a granular medium may have profound differences to conventional thermal noise (*10*), as long as sizable fluctuations exist to activate events, glassy relaxation appears to be universal (*11*, *12*).

In 1989, Edwards and Oakeshott (*13*) proposed the possibility of using the formalism of statistical mechanics to describe the properties of static granular materials. His theory considered as the statistical ensemble the set of static, mechanically stable configurations, which the system acquires after having dissipated the kinetic energy received by repeated perturbation. It set a milestone in the study of granular materials, as it hinted at some order behind the disorder. Since then, many studies (*10*, *14*–*22*) have addressed these questions.

One of these studies is the well-known Chicago experiment (*23*), which presented a simple perturbation protocol able to create such a collection of states. This protocol consists of the repeated application of discrete "taps" to a granular pile confined inside a container, and the collection of static configurations obtained after the system has dissipated the injected energy. For taps with low (fixed) intensities, the system shows a logarithmic increase in density, or packing fraction ϕ, with the number of applied taps (*3*, *10*, *24*, *25*). However, executing a series of stepped annealing protocols, both for increasing and decreasing intensities of the perturbation, the system undergoes a fast "irreversible" transient of low densities and reaches a so-called "reversible regime." There, the density of the static configurations becomes a function only of the intensity of the tap applied. The collection of static configurations at a given tap intensity serves as a setting to test Edwards' hypothesis.

Using a protocol similar to stepwise annealing used in (*23*), but decreasing the tap intensity (represented conventionally by its reduced acceleration Γ) continually between taps at various variation rates ($\dot{\Gamma}$), we have shown (*3*) that the packing fraction ϕ as a function of Γ behaves in a manner resembling the glass transition found in thermal materials (*5*, *8*, *26*, *27*). That is, at high Γ, $\phi(\Gamma)$ evolves independent of $\dot{\Gamma}$, while for lower intensities, it splits into a separate branch for each $\dot{\Gamma}$, reaching higher densities for lower $\dot{\Gamma}$.

Here, we explore the origin of that transition in greater detail, accounting for the heterogeneous response of the system at different heights of the pile to the same tap (*10*, *28*, *29*), as imposed by gravity. As different layers attain different densities along the same protocol and enter a glassy state at different tap intensities Γ, we find that a

[1]Department of Earth Science and Engineering, Imperial College, London SW7 2BP, UK. [2]Department of Physics, Emory University, Atlanta, GA 30322, USA.
*Corresponding author. Email: paulaalejandrayo@gmail.com (P.A.G.); sboettc@emory.edu (S.B.)

grain-level examination of the energy propagation along the system during a tap allows us to collapse the density behavior for the different layers when plotted as a function of the effective energy grains receive from the collective perturbation. In particular, we find a critical value of this effective energy along which the peaks exhibited by the density fluctuations in each layer align.

In effect, we are taking back a step from the macroscopic perspective of Edwards' hypothesis, especially its focus on volume assuming the role of the controlling parameter (*13*) (comparable with temperature in equilibrium statistical mechanics). Instead, we delve into a microscopic analysis of the dynamic process that leads from one static configuration to the next. It opens the door to a first-principles, grain-level characterization of the impact a perturbation has on granular systems, in the spirit of a kinetic theory in statistical physics relating temperature to internal energy. Hence, this microscopic perspective holds the promise to be generalizable to other perturbation protocols (such as seismic or acoustic waves, avalanches, etc.) and to systems with different geometries and grain properties. Although our investigations as of yet fall short in understanding the full impact this effective energy has on transforming configurations, aligning data according to it already explains, e.g., unusual behavior of critical density fluctuations observed previously for the pile as a whole (*17*).

For these insights, we had to perform detailed and extensive molecular dynamics (MD) simulation of soft spheres, in particular using the implementation provided by LIGGGHTS (*30*) open-source software, to record internal energies during the dynamic process and to sample with sufficient statistics for macroscopic variables of static configurations, such as the density and its fluctuations in each layer of the pile.

Figure 1 serves to illustrate the setup for the granular pile used in our MD simulations. Specifically, Fig. 1A presents a series of snapshots of the pile describing the dynamic process during a single tap, after the perturbation has been exerted at $t = 0$ (leftmost panel). The following panels of Fig. 1A show the kinetic energy (color coded from blue for $v = 0$ over white to red for high speeds v) provided by the tap "spreading" through the pile and lastly getting fully dissipated. The dimensionless acceleration Γ is used to represent the tap intensity.

As can be seen from Fig. 1A, the energy imparted by the tap travels along the height of the pile neither in an instantaneous nor homogeneous fashion. Instead, a complex process of energy transfer and dissipation ensues under the influence of gravity that we intend to study in more detail below. It is therefore not unexpected that the granular density of static configurations is often measured over narrow layers of constant height (*23*, *28*, *29*). To measure the packing fraction ϕ, we divide the entire system into 15 cylindrical subregions ("layers"), as schematized in Fig. 1B, stacked along the height of the pile.

In our simulations, we start from a high tap intensity and implement two distinct annealing protocols of decreasing intensity, one continuous and the other stepwise. For the first protocol, three different continuous rates of change were used. The packing fraction ϕ of each layer is measured after each tap. To measure also the density fluctuations $\Delta\phi$, corresponding to the "stationary state" at a given tap intensity, a stepped protocol inspired by (*23*) is performed. In this protocol, we apply a series of taps at each intensity Γ before decreasing it by decrementing the tap amplitude by an amount ΔA. Last, to verify the stationarity and reversibility of the produced states, we repeated the stepwise protocol in the reversed direction, i.e., for increasing intensities.

RESULTS AND DISCUSSION

Local density and its fluctuations

Figure 2 (A to C) shows ϕ as a function of Γ for three $\dot{\Gamma}$ under continuous annealing for each one of the three layers located at the low, middle, and top of the pile marked in Fig. 1B. As previously reported (*3*), within each fixed layer, it can be seen that the data obtained at higher intensities Γ vary together, irrespective of $\dot{\Gamma}$, consistent with equilibrium behavior. However, for lower intensities, they split off into separate branches for different $\dot{\Gamma}$. As a consequence, the final density achieved for $\Gamma \to 0$ becomes a function of the protocol. Remarkably, the regime of Γ where this split occurs itself depends on the layer, suggesting that each strata in the pile transitions into a glassy state at a different tap intensity. Variations in the state between different parts of the pile due to gravity under the same perturbation have been noted previously (*29*). As we will show below,

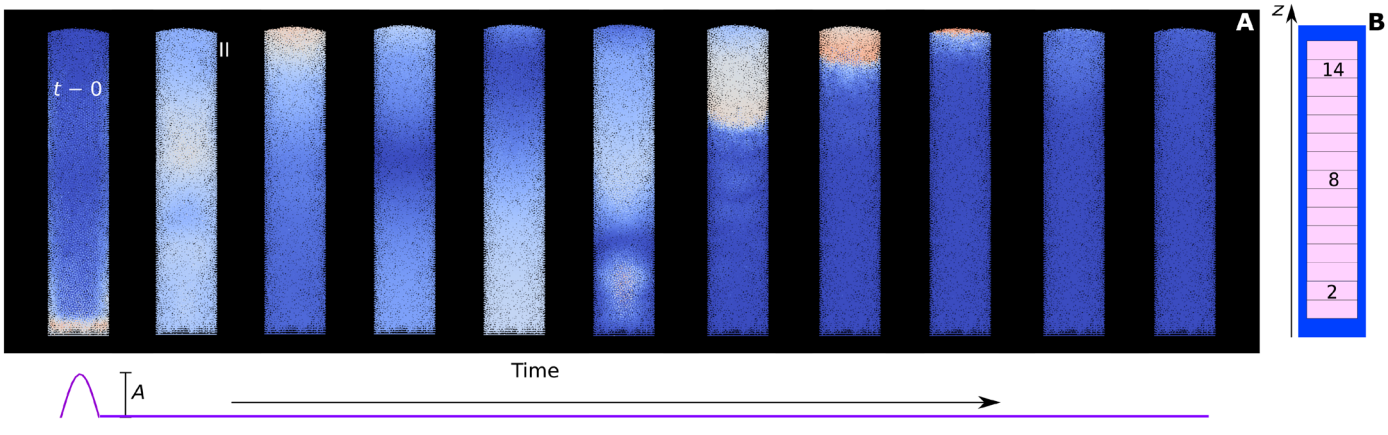

Fig. 1. Evolution of a single tap. (**A**) Snapshots of the cylindrical silo illustrating the pile dynamics during a single tap. At time $t = 0$, the tap is applied (left). The purple line below the snapshots shows the schematic of the corresponding perturbation. The kinetic energy injected traverses the pile (from left to right) until it is fully dissipated through collisions and friction. The color scale reflects the instantaneous speed of each particle, increasing from blue over white to red. (**B**) A schematic of the 15 disk-like subregions (layers) used to measure the local packing fraction, with three representative layers (for low, middle, and top) highlighted for future reference.

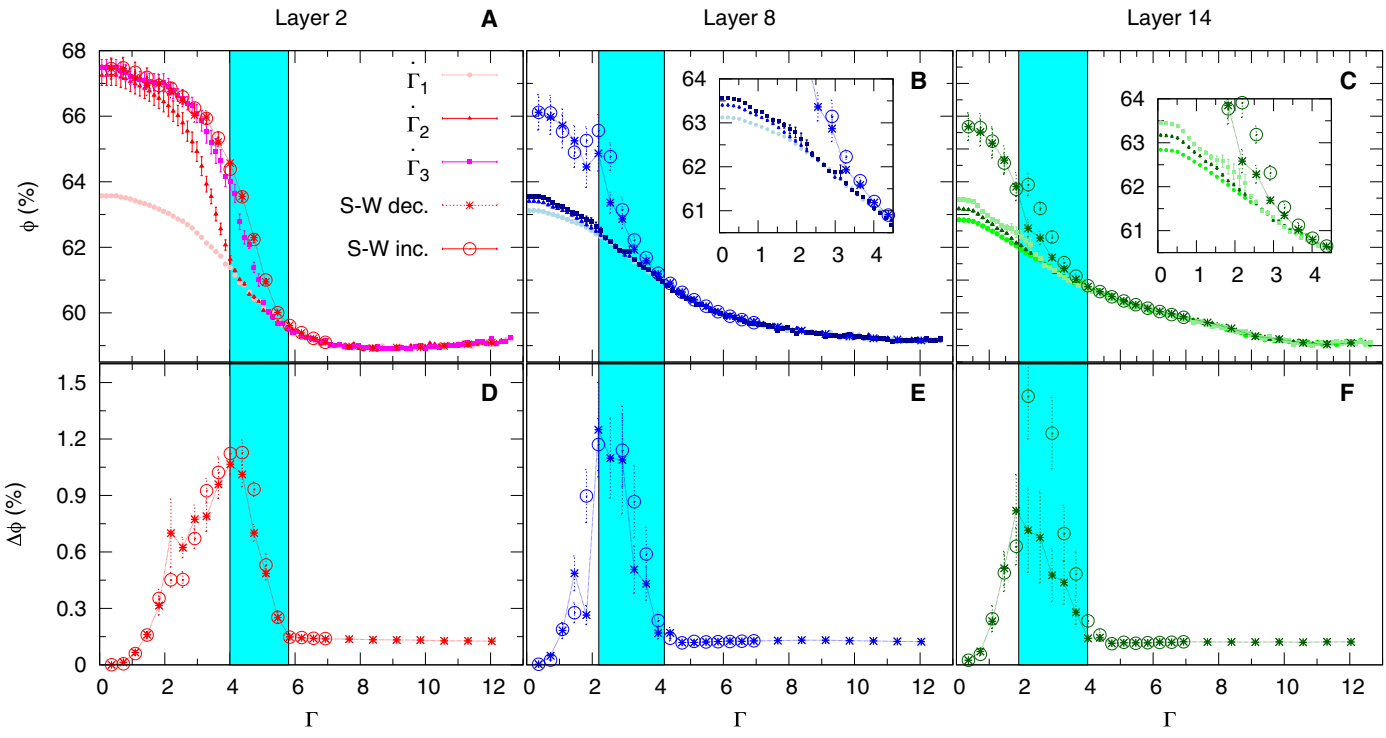

Fig. 2. Packing fraction and density fluctuations in the pile. (**A** to **C**) Packing fraction ϕ as a function of Γ for layers 2, 8, and 14, respectively, located at different heights of the pile, marked in Fig. 1B. For the continuous protocol it is $\dot{\Gamma}_1 = 0.00002\ m(\omega^2/g)$ per tap (red circle), while $\dot{\Gamma}_2 = \dot{\Gamma}_1/4$ (blue triangle-up) and $\dot{\Gamma}_3 = \dot{\Gamma}_1/8$ (green squares). For the stepwise protocol, crosses correspond to the decreasing protocol and open circles to its reverse, i.e., increasing protocol. Insets merely enlarge main plot for $\Gamma < 4$. (**D** to **F**) Density fluctuations $\Delta\phi$ as a function of Γ for the same three layers displayed in (A) to (C), respectively, as obtained by the stepwise protocol. For each protocol, 16 independent realizations were performed, and error bars in all the figures correspond to the SEM. Shaded areas mark the Γ range corresponding to the right slope of each peak in $\Delta\phi$ versus Γ.

these variations can be accounted for by the difference in the effective energy acting in each region.

Also shown in Fig. 2 (A to C) is the density as a function of Γ obtained in the stepwise protocol. As many taps are spent at fixed values of Γ (and many more overall compared to any of the continuous protocols), the densities for this protocol are well converged and provide an upper bound on the faster-moving, continuous protocols. Starting at high Γ, crosses mark the decreasing protocol, while open circles correspond to the same protocol but reversed after the decreasing protocol is completed at $\Gamma \approx 0.37$. Both set of data demonstrate that there is only a minute aging effect on its reversibility that can be ignored for our purposes here.

Focusing on the corresponding density fluctuations $\Delta\phi$ obtained in the stepwise protocol, as shown in Fig. 2 (D to F), we find that irrespective of the direction of the protocol, the fluctuations exhibit identical features as a function of the tap intensity (with small quantitative differences in strength). It can be observed that $\Delta\phi$ as a function of Γ remains almost constant for high intensities until it sharply peaks for lower Γ values, before vanishing as the intensity further decreases. This single-peaked behavior for each layer is consistent with previously reported results (*18*, *28*). However, we note that the right slope of each peak can be associated with the density transitioning into a glassy state, as it corresponds to the regime of intensities (highlighted by a blue stripe) where the splitting takes place in Fig. 2 (A to C) for the respective layer. This behavior is independent of the direction of the protocol, showing that it is a function of the tap intensity and not a results of a residual transient. Thus, although the rise in fluctuations and the onset of glassy behavior are aligned for each layer, neither the intensity Γ of the macroscopic perturbation nor the respective densities, as would be expected from Edwards' hypothesis, allow aligning the data for all layers simultaneously.

Effective energy of grains

To align the onset of glassy behavior between different layers, we now examine in more detail the dynamic process by which each tap distributes energy throughout the system. It permits us to identify an effective energy E_{eff} that quantitatively collapses the transition to glassy behavior for the different layers of the system. In particular, we find a specific threshold value E_c for which particles with $E_{\text{eff}} < E_c$ always assume glassy arrangements, apparently. To this end, we now look at the grain-scale dynamics of the energy transmission and dissipation during the tap.

Figure 3A shows the kinetic energy *ke* per particle [in units of *mgd*] as a function of time during the dynamics. In this example, we used an intermediate tap intensity of $\Gamma \approx 3.65$ and averaged over particles belonging to the three representative layers along the pile. Each exhibits an initial peak, whose value is consistent with $(A\omega)^2/(2gd) \approx 3.65$, the kinetic energy of a particle moving with the maximum speed reached by the perturbation. After this initial peak and a brief period of energy transfer between layers, each layers follows a "free-fall" behavior, decreasing its velocity until near zero before starting accelerating downward and reaching a last peak. It is the value of the last peak in *ke* that interests us, as this is the kinetic

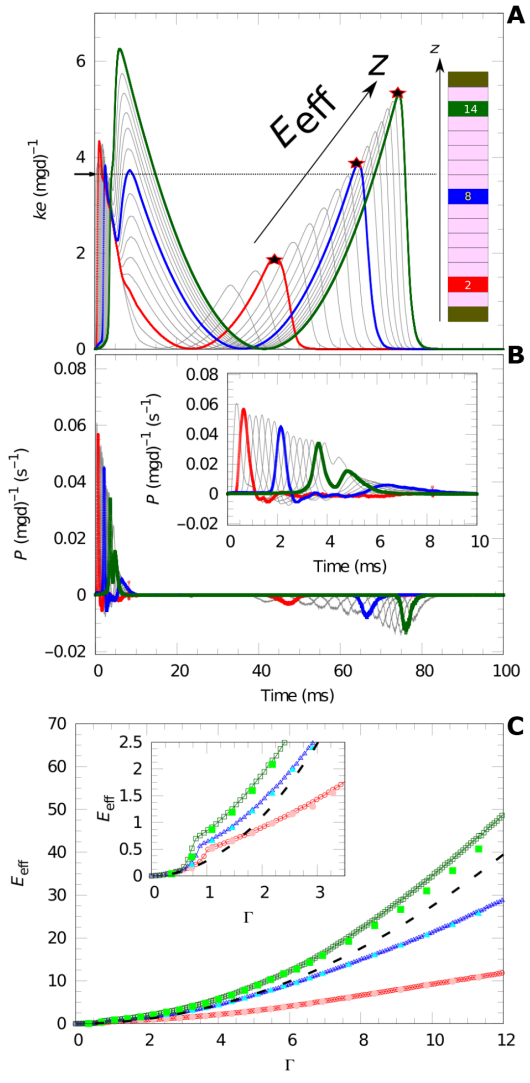

Fig. 3. Energy transfer and dissipation during a tap. (**A**) Average kinetic energy ⟨*ke*⟩ (in units of million gallons per day) for particles during the dynamic process (corresponding to a perturbation of amplitude $A = 0.002$) as a function of time [in color for layers 2 (red), 8 (blue), and 14 (green), as indicated by the stylized height chart in the inset, all other layers indicated in gray]. Initially, for $t = 0$, the tap (almost instantaneously but slightly delayed through the compression of layers below) accelerates particles in each layer upward to the first peak in the kinetic energy, consistent with $(A\omega)^2/(2gd)$ (marked by arrow). Black stars record the effective energy E_{eff} of the last peak that is dissipated by crashing into the layer below. (**B**) Same as in (A) but plotting the corresponding power P in the transfer, gain, or loss, of the total mechanical energy for each layer. (**C**) Relation between E_{eff} and the tap intensity Γ, as experienced by each layer for continuous and stepwise protocols (open and full symbols, respectively). The dashed line marks the relation for the entire pile to behave as a homogeneous solid. The inset shows the enlargement of the low-energy regime most relevant to the glassy behavior, where departure from plain solid behavior is most evident.

energy that particles dissipate when they settle. Marked by a black star, we will call this energy the effective energy E_{eff} that the perturbation imparts to each specific layer. It is easy to see that E_{eff} is an increasing function of the layer height z.

This behavior is corroborated by the transfer, gain or loss, in the total (kinetic and potential) energy per unit time, shown in Fig. 3B. Here, as enlarged in the inset, we note the initial upward acceleration of particles due to the tap, followed by a coherent transfer of energy between layers from the bottom to the top, an effect similar to the "stacked balls demonstration" in introductory physics. The ballistic free-fall behavior leaves the total energy unchanged, which ends with a sequence of layer-by-layer crashes, progressively shorter and more intense, which dissipates the remaining kinetic energy we marked above as E_{eff}.

Figure 3C shows E_{eff} as a function of Γ for the same three layers represented in Fig. 3A. Open symbols correspond to the continuous protocol following Γ_3, while full symbols correspond to the E_{eff} obtained through the stepwise protocol. It can be seen that E_{eff} is largely independent on the protocol followed. A black dashed line represents $(A\omega)^2/(2gd)$, corresponding to the kinetic energy (in units of million gallons per day) that a particle would acquire by moving with the maximum speed reached by the perturbation. The inset in the same figure shows a close-up of the main figure for lower values of Γ. The "kink" corresponds to the intensity at which particles in a given layer stop separating and the system moves as a solid. For example, for the bottom layers, this happens at $\Gamma \approx 1$, as expected for a solid without elastic interactions.

Data collapse as a function of E_{eff}

In the following, we use E_{eff} to collapse our data. To this end, we first consider the stepwise protocol. Figure 4 (A and B) shows ϕ and Δϕ, respectively, for this protocol as a function of Γ, as in Fig. 2 but for all layers simultaneously. Layers 2, 3, 8, and 14 are highlighted by color. From Fig. 4B, we notice that the sharply peaked form of Δϕ as a function of Γ is present in all the individual layers but occurs, however, at different Γ values, as pointed out in Fig. 2. Hence, when measured for the entire pile, these individual peaks in Δϕ add up to form a "trough" as a function of Γ, as shown in the inset of Fig. 4B. This behavior is consistent with previously reported results (*17*, *31*).

Figure 4 (C and D) shows ϕ and Δϕ as a function of E_{eff}, respectively. Figure 4D shows an almost perfect alignment of the peaks of Δϕ as a function of E_{eff}, supporting the hypothesis that E_{eff} is a physically relevant parameter to characterize the state of the system. In particular, we mark $E_{\text{eff}} = E_c \approx 2$ as the effective energy where all fluctuations are simultaneously peaked as the "transition energy." From Fig. 4C, it can be seen that this new parameter (E_{eff}) also aligns the inflection points for the densities ϕ in each layer in the same energy regime as the right slopes of Δϕ.

However, a better collapse for the density in Fig. 4C is hindered by behavior resembling a "finite-size" effect for higher energies, where the data splay out systematically with the height of the layer. Although this residual effect is minor, we attempt to collapse these data further by rescaling with height z, defining the new scaling variable

$$\tilde{E} = (E_{\text{eff}} - E_c)/z \qquad (1)$$

This approach is entirely speculative and violates our desire to avoid system-specific parameters to unify the description. Figure 4 (E and F) shows ϕ and Δϕ as a function of $\tilde{E}$, respectively. While the collapse of the density ϕ in Fig. 4E improves somewhat, the density fluctuations Δϕ become progressively distorted in width for $z \to 0$, see Fig. 4F.

While this result appears to support the existence of a geometric constraint on the dynamics depending on the column height,

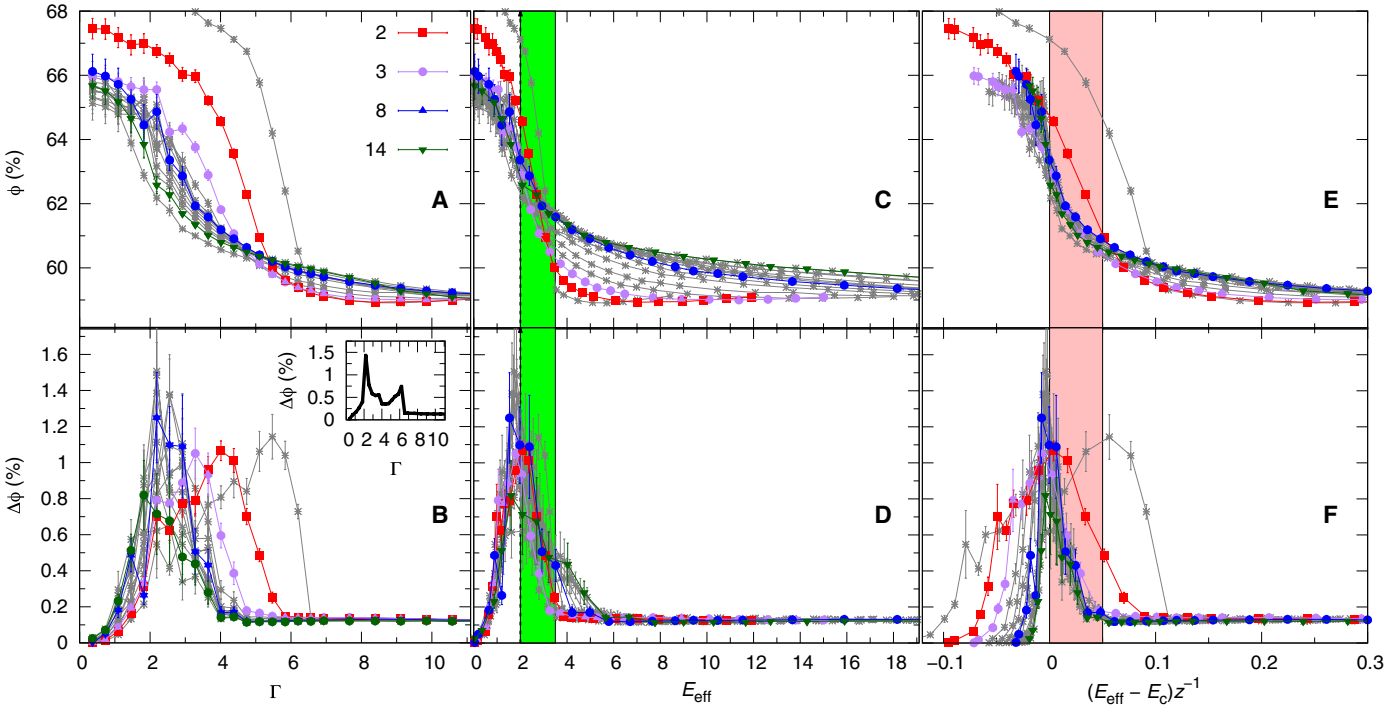

Fig. 4. Data collapse for the stepwise protocol. Plot of the density ϕ (**A**, **C**, and **E**) and density fluctuations Δϕ (**B**, **D**, and **F**) obtained with the stepwise protocol. In (A) and (B), data are plotted as a function of Γ and in (C) and (D) as a function of E_{eff}, measured for different layers along the height of the granular pile. As a function of Γ, different layers behave similarly but are shifted variably, without apparent collapse. When data for Δϕ are averaged over the layers, the individual peaks convolve into a trough, see inset of (B). However, as highlighted in green in (C) and (D), the steep rise in density and the density fluctuations for all layers align when plotted as a function of E_{eff}, revealing the signature of a glass transition (see also Fig. 5). Additional rescaling with the height z of the pile not only improves the collapse in the density in (E) but also stretches the width of the fluctuations at low z.

following the proposal in (*28*, *32*), this dependence could be explained using arguments based on the local expansion between particles mid-flight: From a configuration that would expand homogeneously, particles acquire a speed proportional to their relative height in the pile. Alternatively, this effect could also be associated with the contact network that particles form during flight, as has been discussed before (*20*). There it is shown that the existence of persistent contacts (i.e., contacts that are never broken) during a perturbation is a source of memory in the system. These possible dependencies will be investigated in more detail in future work.

Instead, we summarize all of our data for ϕ in Fig. 5. It demonstrates that there is a common transition into a glassy state occurring in the region of energies corresponding to the right slope of the peak in Δϕ versus E_{eff} (highlighted in light red). Above it, the scaling in Eq. 1 collapses the data for the stepwise and all continuous protocols in all layers simultaneously, whereas for $E_{eff} < E_c$, the data are splitting into separate branches for different annealing rates $\dot{\Gamma}$ and between layers. Thus, the critical value E_c provides a good prediction for the effective energy of particles at the glass transition. In contrast, the inset in Fig. 5 illustrates the breadth over which these transitions spread out for Γ as the controlling parameter, reinforcing the value of our new approach.

In summary, we have shown that the density fluctuations, on approaching the glass transition from higher energies, rise to a sharp

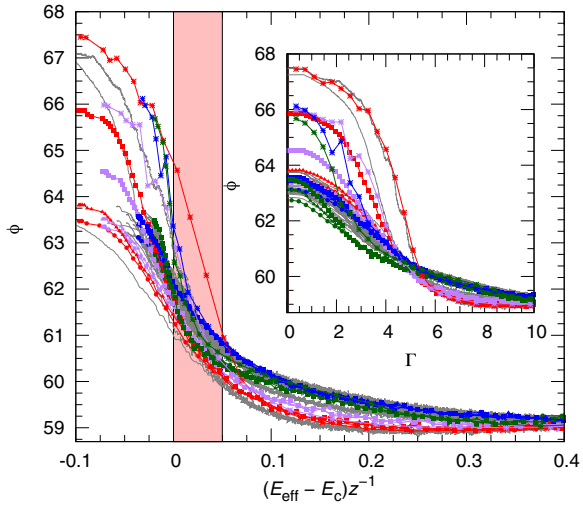

Fig. 5. Data collapse for the continuous protocols. Density ϕ as a function of $\tilde{E}$ (Eq. 1) as obtained for the stepwise (stars) and all three continuous annealing protocols: $\dot{\Gamma}_1$ (circles), $\dot{\Gamma}_2$ (triangles up), and $\dot{\Gamma}_3$ (squares), as well as for all layers [using different colors for the highlighted ones: layer 2 (red), layer 5 (purple), layer 8 (blue), and layer 14 (green)]. Inset shows the same data but as a function of Γ.

peak for each layer of the pile, before vanishing as the perturbation intensity decreases. By analyzing the grain-scale dynamics of the kinetic energy transfer and dissipation during the perturbation process, we have been able to define an effective kinetic energy that allows quantifying the energy of the transition in a unified manner for all layers and intensities. This is a groundbreaking statement, further justified by our ongoing studies on alternate settings discussed elsewhere, as prior experiments and simulations on granular piles were able to agree on qualitative results but struggle to achieve any quantitative comparison within the geometries and parameters they used.

According to Fig. 4, the effective energy merely allows aligning the data but does not achieve by itself a satisfactory collapse of ϕ, hinting at other relevant quantities affecting the transition internally, which we are currently investigating. Although the ad hoc rescaling with the height z reduces the apparent height dependence and produces a rather satisfactory collapse of the density data in Fig. 4E (see also Fig. 5), it unnaturally broadened the density fluctuations for $z \to 0$ in Fig. 4F. Nevertheless, it provides a direction for further investigation into the role of other grain-scale, dynamic parameters, such as the network of granular contacts, or the dependence of the dissipated energy on the mean-free path (due to local expansion and frustration) among the grains. To conclude, we remark that it has been shown that ϕ by itself is insufficient to completely characterize the (static, mechanically stable) configurations of a granular system (*14*, *18*, *19*, *28*, *33*, *34*). For this reason, further work will also have to address the behavior under the scaling provided by E_{eff} for other macroscopic quantities, such as the stress tensor of the system.

MATERIALS AND METHODS

Figure 1 illustrates the setup for the granular pile used in our MD simulations. It consists of a cylindrical silo of diameter $D = 2.4$ cm with 60,000 spherical grains of slightly bi-dispersed diameters [(1 to 1.02) mm in equal number], to reduce crystallization. The height of the granular pile is 12 cm, within a silo whose top (at 60 cm) was chosen high enough to ensure that the grains never interact with it. Within the LIGGGHTS (*30*) open-source software implementation, we also set a friction coefficient of $\mu = 0.5$, a young modulus of $Y = 10^8$ Pa, a restitution coefficient of $\epsilon = 0.5$, a Poisson's ratio of $\nu = 0.3$, and a density of $\rho = 2500$ kg/m^3 for our grains. The initial condition for the pile is obtained by simply pouring the grains into the container.

The tap consists of a half sine-wave $A \sin(\omega t)$ with constant frequency $\omega = (2\pi/0.047)$ Hz, with the amplitude A as the control parameter, applied to the silo by the movement of the entire container (both bottom and side walls). The dimensionless acceleration $\Gamma = A\omega^2/g$, with the gravity acceleration g, is used to represent the tap intensity. Numerically, we consider that the system is static when the kinetic energy of the whole pile drops below a threshold of 10^{-1} J.

Measuring local density of static configurations

To measure the packing fraction ϕ, we divide the entire system into 15 cylindrical subregions (layers), as schematized in Fig. 1B, stacked along the height of the pile from $z = 0.006875$ to $z = 0.11$ m. To reduce boundary effects, particles closer than 2 mm from the silo lateral walls, ≈7mm from the silo bottom, and particles on the surface ($z > 0.11$ m) are disregarded. Each layer defined in this way contains ≈2500 particles.

Three different continuous rates of change were used: $\dot{\Gamma}_1 = 0.00002\,\text{m}(\omega^2/g)$ per tap, $\dot{\Gamma}_2 = \dot{\Gamma}_1/4$, and $\dot{\Gamma}_3 = \dot{\Gamma}_1/8$. The packing fraction ϕ of each layer is measured after each tap. To this end, a Voronoi tessellation (*35*) of the whole system is performed, and the local density of each particle is obtained by dividing its volume by its corresponding Voronoi volume. The densities of those particles whose centers are in the subregion of interest are averaged to obtain the packing fraction ϕ of the corresponding region.

For the stepwise protocol, we decrement the tap intensity by $\Delta A = 0.00004$ m for the first seven steps and $\Delta A = 0.00002$ m for the remaining ones. For this protocol, the selection of the number of taps applied at each given A needed to satisfy the condition of the system reaching the stationary state at that A and to provide enough statistics for an accurate calculation of the density fluctuations. On the basis of preliminary inspection of our data, we found that 500 taps were sufficient. To avoid the transient regime between consecutive intensities, the first 250 taps at each Γ are disregarded. Although this number is overly cautious at high tap intensities, it ensures that we only average over stationary states as the system evolves through its glassy phase. For the remaining 250 taps, we average over ϕ, and $\Delta\phi$ is calculated as the SD of the mean.

Measuring internal energies during the dynamics

To measure the internal energy for each layer of the pile during the dynamics ensuing from the perturbation, we label particles with respect to the layers they reside in for the static configuration before the tap. We then track positions and velocities of all those particles during the dynamic process illustrated by Fig. 1A to calculate the average kinetic and gravitational potential energies per particle for each layer as a function of time. From the decrease in mechanical energy, we can deduce the dissipation particles from the given layer have experienced during the process.

REFERENCES AND NOTES

1. P.-G. de Gennes, Granular matter: A tentative view. *Rev. Mod. Phys.* **71**, S374–S382 (1999).
2. H. M. Jaeger, S. R. Nagel, R. P. Behringer, Granular solids, liquids, and gases. *Rev. Mod. Phys.* **68**, 1259–1273 (1996).
3. P. A. Gago, S. Boettcher, Universal features of annealing and aging in compaction of granular piles. *Proc. Natl. Acad. Sci. U.S.A.* **117**, 33072–33076 (2020).
4. J. M. Hutchinson, Physical aging of polymers. *Prog. Polym. Sci.* **20**, 703–760 (1995).
5. P. G. Debenedetti, F. H. Stillinger, Supercooled liquids and the glass transition. *Nature* **410**, 259–267 (2001).
6. Z. G. Zhu, P. Wen, D. P. Wang, R. J. Xue, D. Q. Zhao, W. H. Wang, Characterization of flow units in metallic glass through structural relaxations. *J. Appl. Phys.* **114**, 083512 (2013).
7. C. B. Roth, *Polymer Glasses* (CRC Press, 2016).
8. U. W. Gedde, M. S. Hedenqvist, *Fundamental Polymer Science* (Springer International Publishing, 2019).
9. P. Sibani, G. F. Rodriguez, G. G. Kenning, Intermittent quakes and record dynamics in the thermoremanent magnetization of a spin-glass. *Phys. Rev. B* **74**, 224407 (2006).
10. E. R. Nowak, J. B. Knight, E. Ben-Naim, H. M. Jaeger, S. R. Nagel, Density fluctuations in vibrated granular materials. *Phys. Rev. E* **57**, 1971–1982 (1998).
11. D. M. Robe, S. Boettcher, P. Sibani, P. Yunker, Record dynamics: Direct experimental evidence from jammed colloids. *Europhys. Lett.* **116**, 38003 (2016).
12. S. Boettcher, P. A. Gago, P. Sibani, Extreme fluctuations driving the relaxation in glassy energy landscapes. *Physica A* **587**, 126522 (2022).
13. S. F. Edwards, R. B. S. Oakeshott, Theory of powders. *Physica A* **157**, 1080–1090 (1989).
14. R. Blumenfeld, S. F. Edwards, On granular stress statistics: Compactivity, angoricity, and some open issues. *J. Phys. Chem. B.* **113**, 3981–3987 (2009).
15. H. A. Makse, J. Kurchan, Testing the thermodynamic approach to granular matter with a numerical model of a decisive experiment. *Nature* **415**, 614–617 (2002).
16. J. G. Puckett, K. E. Daniels, Equilibrating temperaturelike variables in jammed granular subsystems. *Phys. Rev. Lett.* **110**, 058001 (2013).
17. M. Schröter, D. I. Goldman, H. L. Swinney, Stationary state volume fluctuations in a granular medium. *Phys. Rev. E* **71**, 030301 (2005).

18. L. A. Pugnaloni, J. Damas, I. Zuriguel, D. Maza, Master curves for the stress tensor invariants in stationary states of static granular beds. Implications for the thermodynamic phase space. *Pap. Phys.* **3**, 030004 (2011).
19. L. A. Pugnaloni, I. Sánchez, P. A. Gago, J. Damas, I. Zuriguel, D. Maza, Towards a relevant set of state variables to describe static granular packings. *Phys. Rev. E* **82**, 050301 (2010).
20. P. A. Gago, D. Maza, L. A. Pugnaloni, Ergodic-nonergodic transition in tapped granular systems: The role of persistent contacts. *Pap. Phys.* **8**, 080001 (2016).
21. S. Henkes, C. S. O'Hern, B. Chakraborty, Entropy and temperature of a static granular assembly: An ab initio approach. *Phys. Rev. Lett.* **99**, 038002 (2007).
22. E. S. Bililign, J. E. Kollmer, K. E. Daniels, Protocol dependence and state variables in the force-moment ensemble. *Phys. Rev. Lett.* **122**, 038001 (2019).
23. E. R. Nowak, J. B. Knight, M. L. Povinelli, H. M. Jaeger, S. R. Nagel, Reversibility and irreversibility in the packing of vibrated granular material. *Powder Technol.* **94**, 79–83 (1997).
24. P. Sibani, S. Boettcher, Record dynamics in the parking-lot model. *Phys. Rev. E* **93**, 062141 (2016).
25. P. Richard, M. Nicodemi, R. Delannay, P. Ribiere, D. Bideau, Slow relaxation and compaction of granular systems. *Nat. Mater.* **4**, 121–128 (2005).
26. G. L. Hunter, E. R. Weeks, The physics of the colloidal glass transition. *Rep. Prog. Phys.* **75**, 066501 (2012).
27. K. H. Fischer, J. A. Hertz, *Spin Glasses* (Cambridge Studies in Magnetism, Cambridge Univ. Press, 1991).
28. P. A. Gago, D. Maza, L. A. Pugnaloni, Relevance of system size to the steady-state properties of tapped granular systems. *Phys. Rev. E* **91**, 032207 (2015).
29. A. Mehta, G. C. Barker, J. M. Luck, Heterogeneities in granular dynamics. *Proc. Natl. Acad. Sci. U.S.A.* **105**, 8244–8249 (2008).
30. C. Goniva, C. Kloss, N. N. Deen, J. Kuipers, S. Pirker, Influence of rolling friction on single spout fluidized bed simulation. *Particuology* **10**, 582–591 (2012).
31. M. P. Ciamarra, A. Coniglio, M. Nicodemi, Thermodynamics and statistical mechanics of dense granular media. *Phys. Rev. Lett.* **97**, 158001 (2006).
32. L. A. Pugnaloni, M. Mizrahi, C. M. Carlevaro, F. Vericat, Nonmonotonic reversible branch in four model granular beds subjected to vertical vibration. *Phys. Rev. E* **78**, 051305 (2008).
33. S. F. Edwards, The full canonical ensemble of a granular system. *Physica A* **353**, 114–118 (2005).
34. C. C. Wanjura, P. Gago, T. Matsushima, R. Blumenfeld, Structural evolution of granular systems: Theory. *Granul. Matter* **22**, 91 (2020).
35. C. H. Rycroft, VORO++: A three-dimensional Voronoi cell library in C++. *Chaos* **19**, 041111 (2009).

Acknowledgments: These simulation were performed at the Imperial College Research Computing Service (see DOI: 10.14469/hpc/2232). **Competing interests:** The authors declare that they have no competing interests. **Author contributions:** P.A.G. and S.B. designed research, performed research, analyzed data, and wrote the paper. P.A.G. and S.B. contributed equally to this work. **Data and materials availability:** All data needed to evaluate the conclusions in the paper are presented in the paper.

Submitted 27 July 2021
Accepted 22 November 2021
Published 14 January 2022
10.1126/sciadv.abl6304